Research article

Tape surface characterization and classification in automated tape placement processability: Modeling and numerical analysis

Clara Argerich[1], Ruben Ibáñez[2], Angel León[3], Anaïs Barasinski[1,]*, Emmanuelle Abisset-Chavanne[2] and Francisco Chinesta[4]

[1] GEM, UMR CNRS-Centrale Nantes, 1 rue de la Noe, BP 92101, F-44321 Nantes cedex 3, France

[2] ICI Institute, 1 rue de la Noe, BP 92101, F-44321 Nantes cedex 3, France

[3] ESI Group & Bristol Composites Institute (ACCIS), Queen's Building, University Walk, Bristol BS8 1TR, UK

[4] PIMM, ENSAM ParisTech, 151 Boulevard de l'Hôpital, 75013 Paris, France

* **Correspondence:** Email: anais.barasinski@ec-nantes.fr.

Abstract: Many composite forming processes are based on the consolidation of preimpregnated preforms of different types, e.g., sheets, tapes, ... Composite plies are put in contact using different technologies and consolidation is performed by supplying heat and pressure, the first to promote molecular diffusion at the plies interface and both (heat and pressure) to facilitate the intimate contact by squeezing surface asperities. Optimal processing requires an intimate contact as large as possible between the surfaces put in contact, for different reasons: (i) first, a perfect contact becomes compulsory to make possible molecular diffusion at the interface level in order to ensure bulk properties at interfaces; (ii) second, imperfect contact conditions result in micro and meso pores located at the interface, weakening it from the mechanical point of view, where macro defects (cracks, plies delamination, etc.) are susceptible of appearing. As just indicated, the main process parameters are the applied heat and pressure, as well as the process time (associated with the laying head velocity). These parameters should be adjusted to ensure optimal consolidation, avoiding imperfect bonding or thermal degradation. However, experiments evidence that the consolidation degree is strongly dependent on the surface characteristics (roughness). The same process parameters applied to different surfaces produce very different degrees of intimate contact. The present study aims at identifying the main surface descriptors able to describe the evolution of the degree of intimate contact during processing. That knowledge is crucial for online process control in order to maximize both productivity and part quality.

Keywords: surface characterization; curvature; machine learning; ATP composites manufacturing; consolidation; Sparse Proper Generalized Decomposition; nonlinear regression

1. Introduction

Many composite forming processes for manufacturing structural parts are based on the consolidation of preimpregnated preforms, e.g., sheets, tapes, ... Among the numerous technological solutions available, one attracts a lot of interest, the automated tape placement (ATP) due to its versatility and its capacity to avoid the use of autoclave.

In this process a tape is placed and progressively bonded to the substrate consisting of the tapes previously laid-up. The cohesion of two thermoplastic layers requires specific physical conditions: an almost perfect contact (intimate contact) and a temperature enabling molecular diffusion within the process time window, while avoiding thermal degradation. Because the characteristic low thermal conductivity of usual resins, an intense local heating is usually considered (laser, gas torches, ...) in conjunction with a local pressure applied by the consolidation roller moving with the heating head, as illustrated in Figure 1.
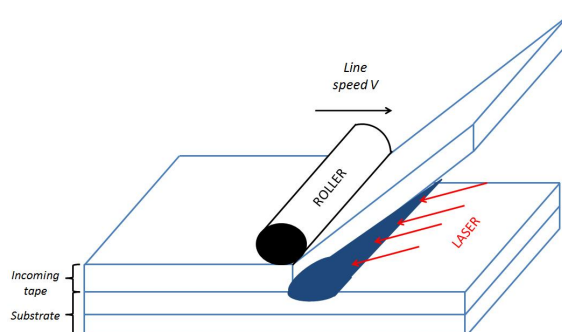
Figure 1. Sketch of the automated tape placement (ATP).

The numerical model of this process was addressed in [1] by using advanced numerical techniques, the so-called Proper Generalized Decomposition (PGD) [2–6]. The separated representation involved in the PGD enables the 3D high-resolution solution of models defined in degenerated domains where at least one of their characteristic dimensions remains much smaller than the others [7–10] and also constructing solutions of parametric models where the model parameters are considered as extra-coordinates [11].

Consolidation requires supplying heat and pressure to ensure the intimate contact at the plies interface. That intimate contact is required to promote the molecular diffusion. In this process heat plays a double role, on one hand it enhances molecular mobility and on the other hand, the decrease of the material viscosity with the temperature increase, facilitates the squeeze flow of the heated asperities located on the ply surfaces under the compression applied by the consolidation roller.

Many studies in the past considered the squeezing of asperities under the action of an external applied pressure, using different representations of rough surfaces [12, 13]. The characterization of random surfaces and the effect of roughness on physics defined at the surface level is a recurrent issue widely addressed in many works [14–21]. Fractals have been largely considered for describing these random surfaces exhibiting self-affinity through many space scales [22–30].

In our recent works, we addressed the asperities squeezing considering both linear and nonlinear fluid constitutive equations. Instead of using rectangular representations of asperities [12, 13] we considered in [31, 32] a fractal surface representation, taking into account the roughness anisotropy

that pre-impregnated composites exhibit. However, fractal representations were unable to explain experimental findings, in particular surfaces having the same fractal parameters could exhibit different behavior during consolidation. This issue comes directly from the definition of the fractal parameters, which are not sufficient to define unequivocally a surface from the point of view of consolidation purposes. Indeed, definitions including more geometrical scales will be required to complete the definition of a surface. This may result in two different surfaces having the same fractal parameters and under the same process conditions exhibit at the end different consolidation degree. To alleviate those limitations a description of the real surface based on a wavelet-based multiresolution approximation was proposed in [33], on which squeezing flow operates enabling the quantification of consolidation. Different real surfaces were analyzed, and the effect of the different material and process parameters on the reached degree of consolidation was pointed-out. Squeezing hypotheses consisting in assuming a plate surface that compresses the other surface which state is a sum of the roughness of both surfaces in contact [34].

As indicated, the analyses performed in [33] concerned the effect of the material and process parameters on the evolution of the degree of intimate contact, however an important, even major, question remains unsolved, the one concerning the effect of the parameters related to the surface description itself.

The present study aims at identifying the main surface descriptors able to characterize the evolution of the degree of intimate contact during processing. That knowledge is crucial for online process control in order to maximize both productivity and part quality. For that purpose, we discuss in the next sections different surface descriptors, the consolidation modeling as well as different strategies of meta-modeling, in particular tree-based and sparse PGD based regressions. Then, a simulation of the ATP process is performed on a set of real surfaces and the output of interest, the intimate contact, is expressed from few geometrical parameters describing the surface with respect to the physics considered (here the heating and squeeze flow). Both modeling approaches are then compared and numerically validated.

A real experimental validation remains a tricky issue. In [35] authors follow and visualize the surface squeezing by compressing a thermoset pre-impregnated tape with a rigid transparent plate. However, the rheological behavior of thermoset and thermoplastic materials are quite different, the last exhibiting a significant shear rate and temperature dependence. On the other hand, we proved in our former work [34] that squeezing a surface with a rigid plane plate is quite different of mutual squeezing induced by the contact between two rough surfaces. Thus, in our works (in progress) we are considering the contact and compression of two rough thermoplastic surfaces, using thermostated plates. By stopping the compression at different times, and then to cut and to examine the cross section, and in particular the interface between both tapes. The process is quite expensive in time and ressources, and being destructive (one cannot follow the same sample during the whole compression test) requires a statistical analysis. The associated results and analysis results will be reported in forthcoming publications.

2. Materials and methods

As just discussed two main physical phenomena must be considered when modeling ATP processes: heating and asperities squeezing. Both were extensively addressed in our former works [31–33]. In

what follows and for the sake of completeness we summarize the main components of the modeling approach related to the real surface representation and the associated squeezing flow.

2.1. Multi-scale modeling of pre-impregnated tape surfaces

The main advantage of characterizing a real surface by using the Haar wavelets is that these having a rectangular form, they allow representing any real surface as a sequence of rectangles of different height and width. This representation is very convenient as discussed later for simulating the surfaces squeezing. The use of wavelet-based multi-resolution analysis combined with the Proper Generalized Decomposition was addressed in [36] and will be used in a similar context in the present work. Interested readers can refer to it and the references therein.

For the sake of clarity Figure 2 depicts the multi-resolution wavelet representation of a simple profile, where different levels of representation can be observed. When using multi-resolution analysis, the representation levels become embedded, that is, the solution at a certain level contains the ones at the lower levels and it is contained in the greater levels representations. The higher the level is, the smaller the support (width) of the Haar function, allowing for better resolutions. Thus the real surface profile can be represented with the required accuracy by choosing an adequate level of approximation.
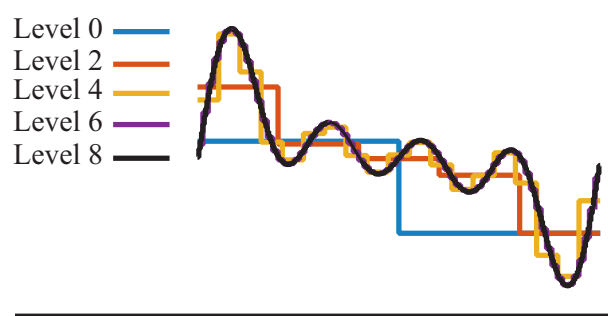
Figure 2. Simple surface representation using Haar wavelets.

In multi-resolution analysis each level can be written from the previous one by adding its orthogonal complement. When this orthogonal complement becomes small enough, one can consider that the function is adequately represented. Such kind of representation, composed of rectangular elements, is very favorable in a double sense: (i) it facilitates a space separated representation within the PGD framework for performing high-resolution thermal analyses [32]; and (ii) it allows addressing the squeeze flow within the lubrication approximation that instead of solving a problem involving the velocity field in a 3D domain (at each squeezing step), solves a problem involving the pressure field in a 2D domain and at each squeezing step, as described below. Moreover when using the PGD in 2D domains, the solution procedure results in a sequence of 1D problems as described later.

2.2. High-resolution thermal analysis

When considering, as just discussed, the surface represented by a sequence of rectangular elements, high resolution thermal simulations can be performed within the Proper Generalized Decomposition (PGD) framework by transforming the 2D heat conduction problem (defined in cross section of the

layered stacking composed of the already consolidated tapes and the one under consideration) into a sequence of 1D heat transfer problems along directions y (width) and z (thickness) when assuming a separated representation of both the temperature field and the material thermal properties. For more details about the method, the reader is referred to [32].

The reduction of a 2D problem into a sequence of 1D problems is compulsory if fine details related to the multi-scale surface representation are retained in the simulation for describing very accurately the evolution of the degree of intimate contact and molecular diffusion at the interface where contact applies.

Within the PGD framework the temperature $T(y, z)$, is searched in the separated form

$$T^n(y, z) \approx \sum_{i=1}^{M} Y_i^n(y) Z_i^n(z), \tag{1}$$

where the super-index $\bullet^n$ refers to the n-th time step, that is $t = n\Delta t$, and the thermal properties, in the present case, the thermal conductivity and specific heat capacity, are also expressed using a separated representation [32].

The transient thermal problem, using the notation $\mathbf{x} = (y, z)$, is defined in the 2D rectangular domain Ω illustrated in Figure 3, and reads

$$\rho C_p \int_\Omega T^* \frac{\partial T}{\partial t} d\mathbf{x} - \int_\Omega T^* \nabla \cdot (\mathbf{K}(\mathbf{x}) \nabla T) \, d\mathbf{x} = 0, \qquad \forall T^* (\mathbf{x}) \tag{2}$$

with the initial temperature given by $T(\mathbf{x}, t = 0) = T_{amb}$, T_{amb} being the ambient temperature. On the lateral boundaries thermal exchanges with the surrounding air assumed at ambient temperature are enforced. On the bottom surface the heat flux from the part to the tool is expressed from a different exchange coefficient and finally on the top boundary the exchange applies with the roller when it compresses the surface and with the surrounding air. Moreover, thermal conduction between the different plies constituting the substrate is affected by a contact thermal resistance as discussed in our former works [1].
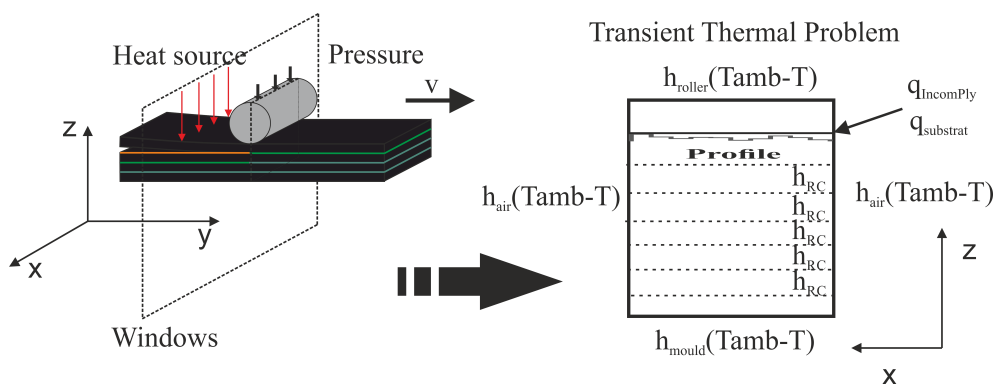
Figure 3. Computational model.

Because the thermal model is coupled with the squeeze flow occurring when the roller compresses the incoming tape, the interface evolves and then the separated representations of the thermal properties must be updated.

The importance of fine enough thermal solutions is twofold. First the temperature determines the resin viscosity of major importance when simulating the squeeze flow at the interface level, the last determining the evolution of the intimate contact and then the thermal flux across it. Second, the thermal field affects the resin rheology and the resin flow at the interface level, and the last determines the heat flux across the interface and then the thermal field evolution.

2.3. Surface evolution during the in-situ consolidation

As commented before, the surface is expressed using Haar wavelets, leading to a multi-scale representation that approximates the surface using rectangular elements. This representation is well adapted to the lubrication hypotheses. In the case of a prepreg surface, the height is very low with respect to the width of the domain, at least one order of magnitude, validating the lubrication hypotheses. The squeeze flow of a rectangular element was considered in many works, and here we consider the assemblage of such elements, assumed representing up to a certain level of accuracy the real surface. The surface is assumed as a succession of fluid columns. Those columns will be compressed from top to bottom according to a squeeze flow model, and the compressed volume will move towards the neighboring fluid elements.

We define the "crushing time" as the one needed for reaching a perfect degree of intimate contact. In what follows, different surfaces will be compared according to their associated crushing times.

2.4. Surface descriptors

Roughness parameters were considered in many works [37–39]. ISO 16610-21 addresses surface analysis by differentiating waviness (associated to the macro-scale) and roughness (related to the micro-scale). A gaussian filter (as ISO 16610-21 recommends) is considered for that purpose. Thus, if Z represents the height of a generic surface, the ones related to the waviness and roughness are denoted respectively by Z_w and Z_r, according to

$$Z = Z_w + Z_r. \tag{3}$$

Figure 4 depicts for six profiles extracted from a prepreg, their macro-scale waviness and micro-scale roughness. Before extracting these two surface descriptors, we calculated the height average of all the available surfaces (population height average), and then for each one of the surfaces, we first remove its own height average and then add the population height average to avoid biased behaviors induced by different height averages of the different surfaces.

Inspired by the fact that most of diffusive transport phenomena are induced by curvature, we consider in the present work the curvature of the surface where the squeezing flow occurs as a potential descriptor of the surface with respect to the crushing time. Intuitively we can visualize low curvature as large plateau of the surface topography. Squeezing a large plateau under the effect of the applied pressure seems difficult because all the material must flow. On the contrary, a surface exhibiting high curvature can be visualized as having many thin pics, that when compressed easily flows to fill the neighbor valleys, as sketched in Figure 5. In this figure the upper image represents a thin column of fluid being squeezed and the required force. In the lower image a wider column of fluid is represented and a higher squeezing force required. For a surface this means, the wider a peak, the more difficult to squeeze it. The Haar wavelet representation here considered for representing the

surfaces does not allow calculating its second derivative that vanishes or becomes infinite, thus a simple finite difference is applied at each node considering an average value of the surface height at nodes where the surface height becomes discontinuous.
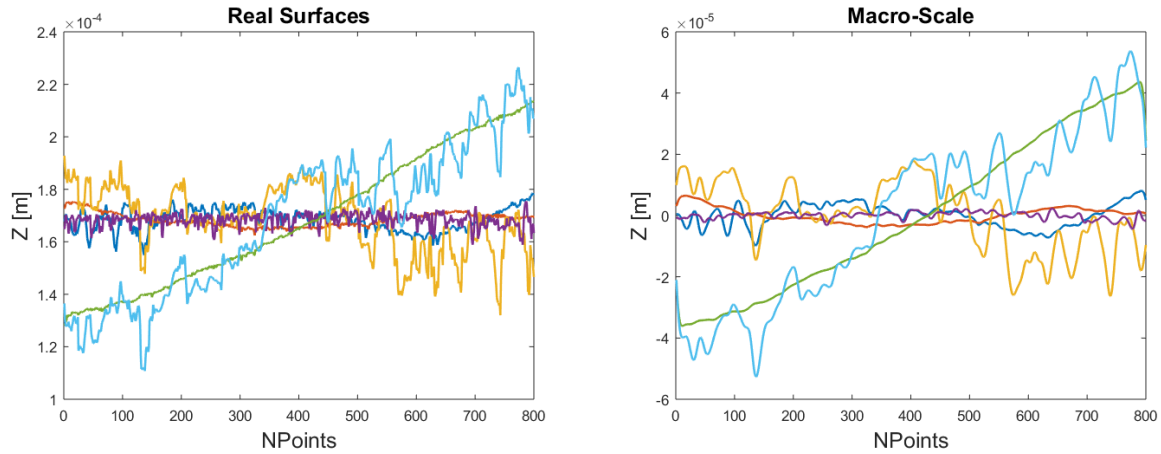
(a) Profiles of six real surfaces

(b) Macro-scale waviness (100 points correspond to 350 micrometers)
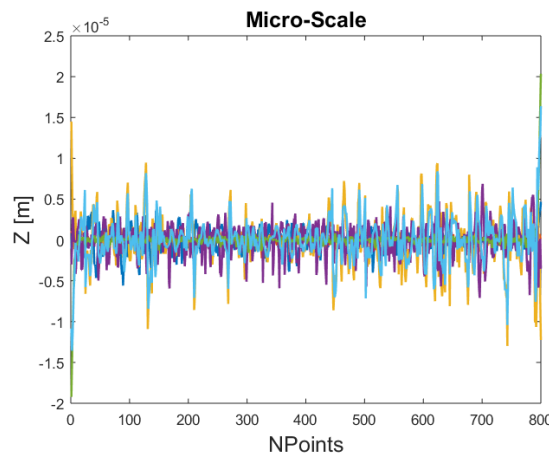
(c) Micro-scale roughness (100 points correspond to 350 micrometers).

Figure 4. Differentiating waviness and roughness of six real surfaces.

For better quantifying the size effect we consider at time t the rectangular domain representing an asperity $\Omega_t = [-L_t/2, L_t/2] \times [-H_t/2, H_t/2]$ occupied by a Newtonian fluid characterized by a viscosity η, with, $L_t \gg H_t$. This element results from the compression of the initial rectangular element $\Omega_0 = [-L_0/2, L_0/2] \times [-H_0/2, H_0/2]$, with $H_t L_t = H_0 L_0$ ensuring the fluid incompressibility. We assume that on the upper boundary $z = H_t/2$ a normal force F is applied. The associated compression rate will be noted by W (see Figure 6). Assuming lubrication flow conditions, the applied force and the compression rate verify the relation,
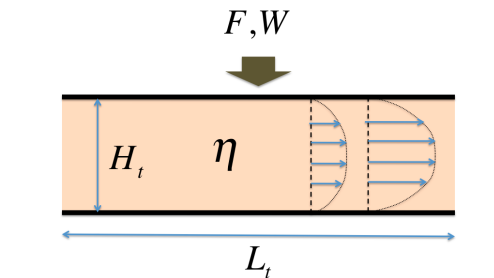
$$F = \frac{W\eta L_t^3}{H_t^3}, \tag{4}$$

where F is the force per unit depth. This proves that for the same compression rate and thickness

evolution, for a larger asperity (higher L_t), a bigger Force F would be needed, or equivalently, the same force squeezes faster thin asperities.
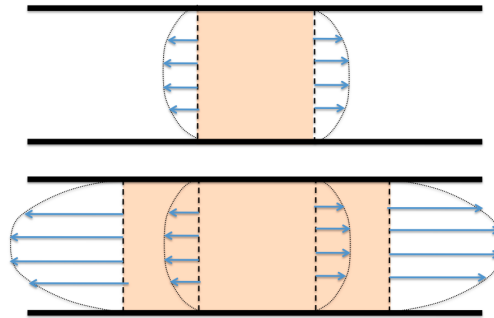
Figure 5. Squeezing rectangular fluid volumes representing asperities of different length.

Figure 6. Squeezing a rectangular fluid volume representing an asperity.

Thus, curvature seems to be a key parameter describing the surface and with a clear physical content in what concerns the squeezing flow leading to intimate contact. However, that curvature can be present, in real surfaces, and more particularly in pre-impregnated composites, at different scales. Thus, in what follows we will consider the curvature associated with both the macroscopic waviness and the microscopic roughness, and it is expected the former, associated with larger space scales, controlling the squeezing dynamics. Intuitively one expects optimal consolidation to be associated with negligible macro-curvature and very high micro-curvature.

Other than the curvature we also consider other potential geometrical parameters: the volume of fluid as well as the slope (first derivative of the surface profile) at both the macro and micro scales. Those parameters are expressed from:

- Macro-slope: Z'_w, with $\bullet'$ the first derivative.
- Macro-curvature defined from the standard deviation of the Z''_w according to

$$\kappa_w = \left| \frac{\sigma(Z''_w)}{\sigma(Z_w)} \right|, \tag{5}$$

where σ refers to the standard deviation, and $\bullet''$ the second derivative.
- Micro-slope: Z'_r.

- Micro-curvature

$$\kappa_r = \left| \frac{\sigma(Z_r'')}{\sigma(Z_r)} \right|. \tag{6}$$

- The normalized volume of fluid

$$A = \frac{\int Z dy}{\mathcal{A}_{max}}, \tag{7}$$

with $\mathcal{A}_{max}$ the maximum value of A for the different considered surfaces.

In what follows, and from these tentative set of parameters, we are trying to express the dependency of the crushing time with respect to the surface geometry, the last described from the above parameters. For that purpose, first we consider data-mining techniques, in particular "decision trees" (freely available in several softwares), due to its ability to classify and to generate regressions. Thus, on one hand we expect to understand the relevance of these parameters, their relative significance, and on the other hand, after validating its relevance and completeness ans for any other surface described from these geometrical parameters, estimate the crushing time.

An alternative strategy for generating such a transfer function relating the crushing time and a set of geometrical parameters easily accessible and allowing a non ambiguous determination of the output of interest (i.e., the same parameters cannot be associated with different values of the output), consists of defining a multidimensional polynomial relating both, inputs (geometry) and output (consolidation indicator, here the crushing time). However multidimensional interpolation or approximation can suffer of the so-called curse of dimensionality. In order to circumvent, or at least alleviate that illness, authors recently proposed to use a separated representation based approximation, a sort of nonlinear regression based on the use of a sparse Proper Generalized Decomposition described in the next section.

2.5. *Nonlinear regression based on the use of sparse PGD (sPGD)*

We consider for the sake of simplicity a two-dimensional function $f(x, y)$ only known at few locations $\mathbf{x}_i = (x_i, y_j)$, $i = 1, \cdots, P$, of the parametric space $(x, y) \in \Gamma$.

The sPGD looks for a separated function $u(x, y)$ of the target function $f(x, y)$,

$$u(x, y) = \sum_{i=1}^{\mathrm{I}} X^i(x) Y^i(y), \tag{8}$$

under the constraint

$$\int_\Gamma w^*(x, y)\, (u(x, y) - f(x, y)) d\mathbf{x} = 0, \quad \forall w^*. \tag{9}$$

However the integral above cannot be directly used because function $f(x, y)$ remains unknown everywhere except at the measurement points $\mathbf{x}_i$. Thus, one possibility consists in adopting a Petrov-Galerkin formulation where the previous integral reduces to a simple collocation at points $\mathbf{x}_i$, $i = 1, \cdots, P$. For that purpose it suffices considering as weighting functions $w^*(\mathbf{x})$

$$w^*(\mathbf{x}) = u^*(\mathbf{x}) \sum_{i=1}^{P} \delta(\mathbf{x}_i), \tag{10}$$

with $\delta(\bullet)$ the Dirac distribution.

Then the solution process, i.e., the construction of the separated representation begins, and proceeds as described in the third chapter of [4]. A couple of important remarks are:

- When using the standard greedy constructor (alternate directions fixed-point schema) functions $X_i(x)$ and $Y_i(y)$ are computed in a decoupled manner, and consequently a reduced data-set P allows a quite rich polynomial approximation of both unknown functions X_i and Y_i, much richer than expressing $u(\mathbf{x})$ using a full dimensional polynomial (2D in the present example).
- As the points distribution can be quite irregular, to avoid oscillations of the one-dimensional approximations of both X_i and Y_i, more stable approximations based on kriging were considered. Kriging-based interpolation is based on the assumption that the interpolated variable consists of a Gaussian process with "a priori" chosen covariance. Here for improving the smoothness of PGD modes and the convergence of the separated representation constructor, we start with a smooth approximation for the first mode, then after convergence, we increase the approximation degree (kriging control points) and so on. This adaptive strategy enhances the constructor efficiency.

3. Thermal analysis

As previously discussed consolidation depends on heating and squeezing. Both are assumed depending on the same surface geometrical parameters. Thus, first, we analyze the dependence of the heat flux for the four surfaces depicted in Figure 7 and for four squeezing degrees: 0%, 25%, 50% and 75% (Figure 8).
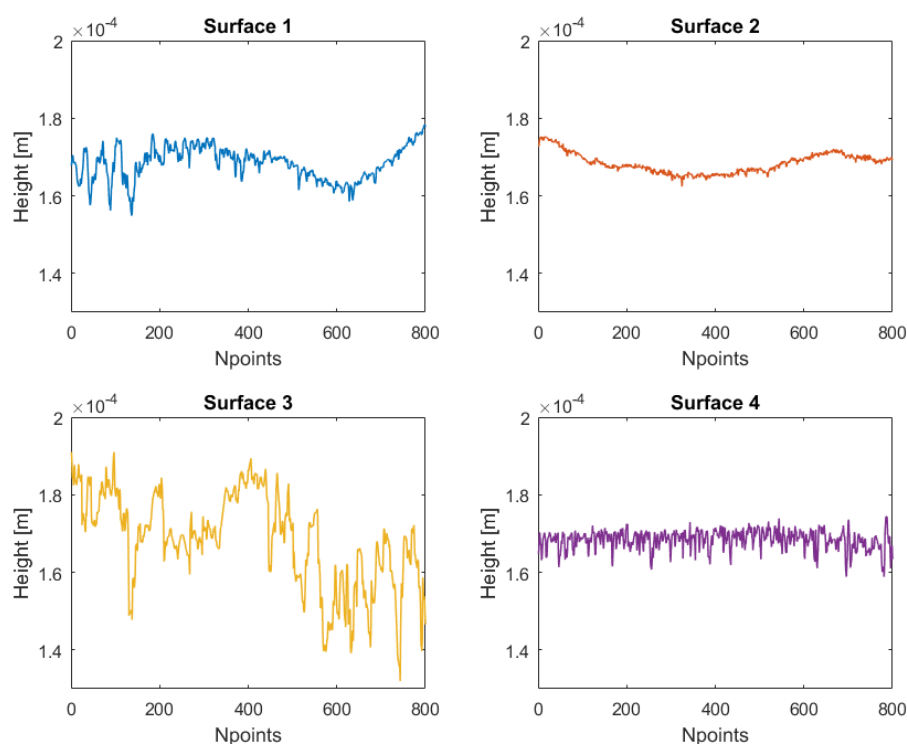
Figure 7. Surfaces considered in the thermal analysis.
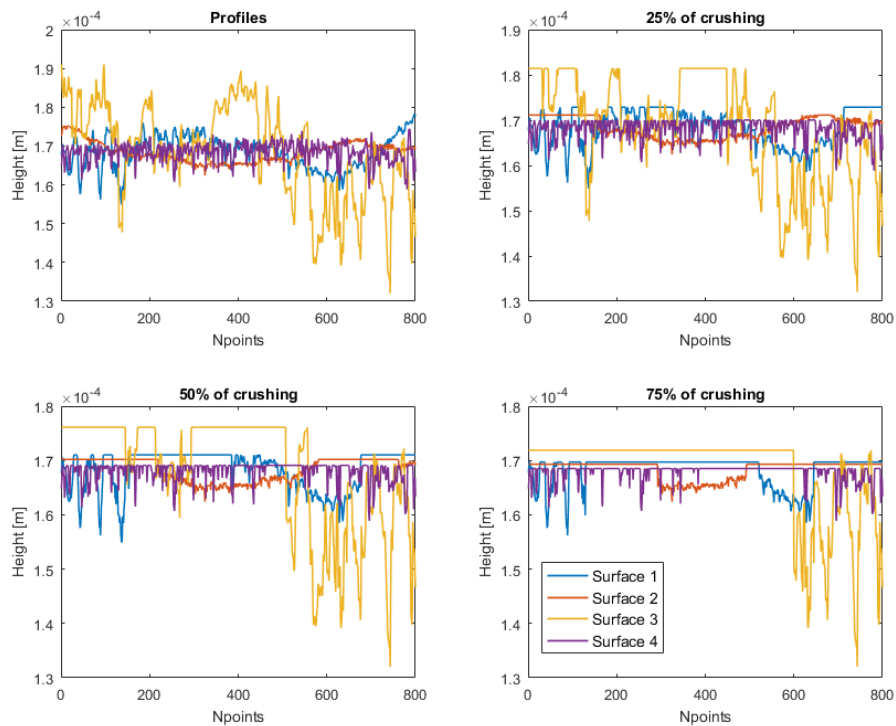
Figure 8. 0%, 25%, 50% and 75% squeezed surfaces.

We apply a difference of 100 degrees between the top and bottom plates, solve the heat transfer equation by using the material $K_m = 0.5$ (units in the metric system) and air $K_a = 0.024$ conductivities, and from that the heat flux at the bottom plate, and finally integrate the last on the bottom surface.

Figure 9a depicts the evolution of the area of intimate contact of the 4 surfaces with the squeezing degree. The other images in Figure 9 represent the heat flux, the macro and micro-curvatures for each of the four surfaces during their squeezing.

In the analysis of the results we consider Surface 1 as reference because its micro and macro curvatures are close to the average of those of the four surfaces. Surface 2 exhibits lower macro and micro curvatures while Surface 3 has higher micro and macro curvatures. Finally Surface 4 has a similar macro-curvature than the reference surface (Surface 1) but presents a higher micro-curvature.

The analysis of results depicted in Figure 9 leads to the following conlusions:

- *Surface 1:* Considered as reference.
- *Surface 2:* The wished lower macro-curvature is compensated by the lower micro-curvature and consequently the behavior remains quite close to the one that the reference surface exhibits.
- *Surface 3:* Here the higher macro-curvature has as expected a very negative impact on the heat transfer.
- *Surface 4:* In this case being the macro-curvature similar to the one of the reference surface, the behavior is expected being mostly governed by the micro-curvature that being larger facilitates the heat transfer.

In order to confirm the just argued mechanisms, we perform a coupled analysis (thermal and

squeezing flow) of a large set of real surfaces and use advance modeling approaches (data-mining and nonlinear regression).

(a) Intimate contact

(b) Heat flux

(c) Macro-curvature

(d) Micro-curvature
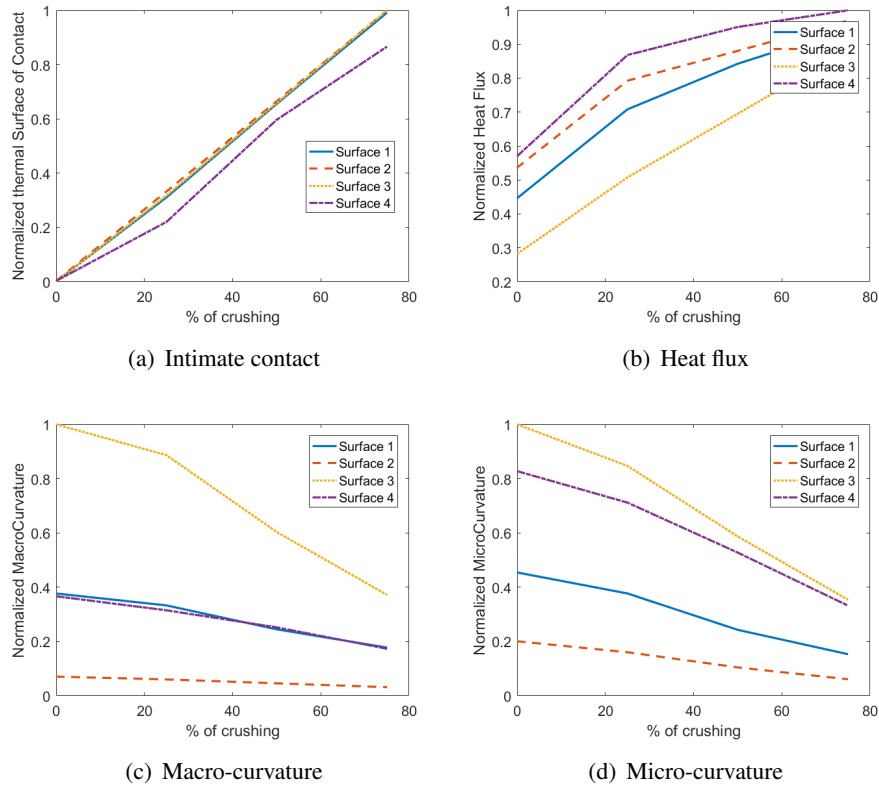
Figure 9. Squeezing induced evolution of different parameters.

4. Consolidation modeling

We consider a set of $M = 1359$ surface profiles extracted from 16 real different pre-impregnated composite parts, and run an ATP simulation on each profile to obtain the time evolution of the intimate contact. These 16 pre-impregnated composites covers the whole market: different customers, different impregnation procedures, ... and then allow to derive valuable conclusions. For each pre-impregnated composite, a number of samples large enough was considered, between 80 and 90 samples, to ensure the validity of statistical analysis.

The analyzed profiles and the time evolution of the intimate contact are depicted in Figure 10.

4.1. Analysis by using decision trees based regression

The data-set consisting of the crushing time (the one at which an almost perfect contact is attained) and the 5 geometrical parameters previously introduced (micro and macro curvatures, micro and macro slopes and volume of material) was used to create the searched regression relating the crushing time with the surface geometrical parameters. Figure 11 depicts the obtained results where it can be noticed that as expected the macro-curvature appears as the most relevant parameter for explaining

processability. The obtained regression has a reliability of 91.43%, that correspond to the expected success when predicting the target.
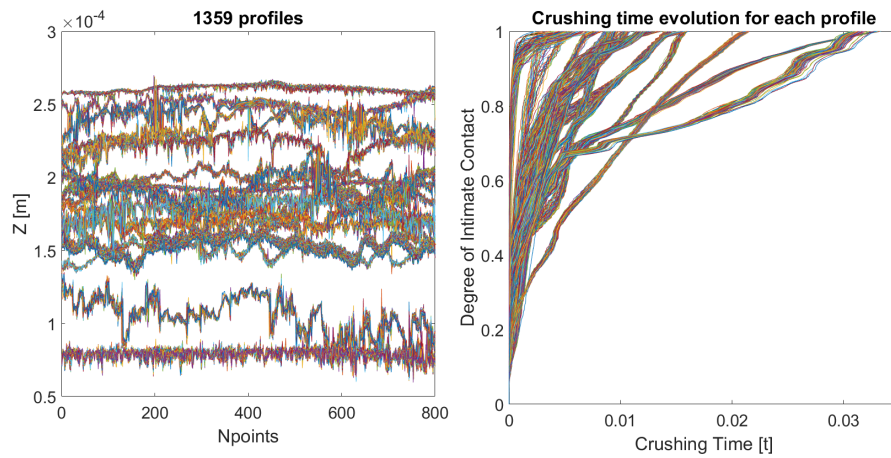
**Figure 10.** Analyzed surfaces and their crushing time evolution.
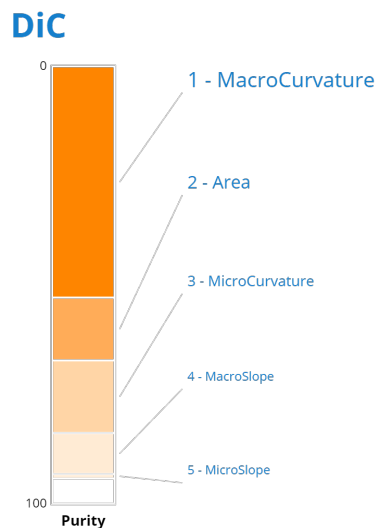
Figure 11. Parameters weight for explaining the degree of intimate contact.

To validate the procedure, a tree-based regression was performed by using a part of the available data (training data), and then comparing the predictions with the data for the remaining surfaces. In order to quantify the predictive capability we define the error ϵ

$$\epsilon = \sqrt{\sum_{i \in \mathbb{S}} \frac{\left(t_i^{ref} - t_i^{est}\right)^2}{\left(t_i^{ref}\right)^2}}, \tag{11}$$

where $\mathbb{S}$ is the set of surfaces that were not involved in the regression model construction, and t_i^{ref} and t_i^{est} are respectively the reference crushing time (obtained by simulating numerically the squeezing process) and the one estimated by using the regression model, both related to each surface $i \in \mathbb{S}$.

Figure 12 shows the evolution of error ϵ for estimating the crushing time depending on the number of surfaces used to build the regression tree. As expected, this error decreases by increasing the number of surfaces used for the model training. It can be noticed that the error reaches a plateau (of about 4%) when considering more than 40% of the available surfaces in the regression construction.
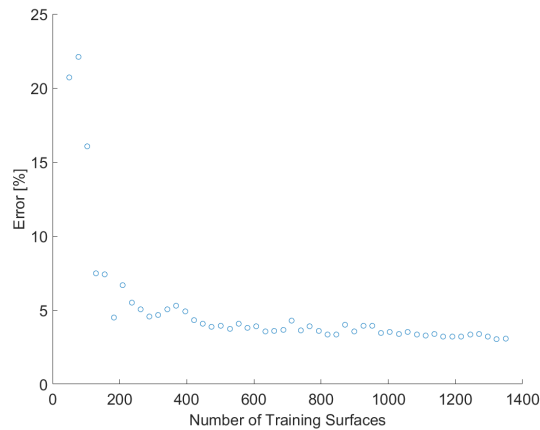
Figure 12. Error versus number of surfaces considered for defining the tree-based regression.

4.2. sPGD-based nonlinear regression

This section aims at comparing the tree-based regression with the one obtained by using the sparse Proper Generalized Decomposition (sPGD) previously introduced. The main advantage of the last is its versatility and its physical foundations. Moreover, it becomes fully combinatorial with respect to tree-based regression in which the curse of dimensionality was circumvented by defining a sequence of the different branches constituting the tree.

Manifold learning allows clustering surfaces with respect to the output of interest, here the crushing time, as Figure 13 reveals, where color is related to the magnitude of the crushing time. For the sake of clarity we considered three of the five involved parameters for the representation.

Now, the sPGD looks for approximating the crushing time C_t depending on the five selected parameters: κ_w, κ_r, Z'_w, Z'_r & A; in the separated form

$$C_t(\kappa_w, \kappa_r, Z'_w, Z'_r, A) \approx \sum_{i=1}^{C} F_i^1(\kappa_w) F_i^2(\kappa_r) F_i^3(Z'_w) F_i^4(Z'_r) F_i^5(A), \qquad (12)$$

where the so-called modes F_i^k, depending on the different parameters, are approximated as previously discussed by using 1D-kriging.

The solution obtained by using the sPGD is then compared to the one resulting from tree-based regression, using the error indicator ϵ previously introduced in Eq (11) when considering 50% of the surfaces for constructing the model.

Figure 14 depicts the evolution in the predictions obtained from the sPGD depending on the number of modes considered in the PGD separated representation. Stars represent the error for the surfaces that served to construct the approximation, that is not zero because the considered approximation (using

12 kriging control point in each direction) is unable to fulfill a perfect interpolation of all the training points. Circles are used when considering all the surfaces, and as expected it is a bit higher than the previous one (that only considered the surfaces used for constructing the nonlinear sPGD-based regression). However, the error gap is quite small, and as in the case of the tree-based regression, the error related to the sPGD approach stagnates around 5% error.
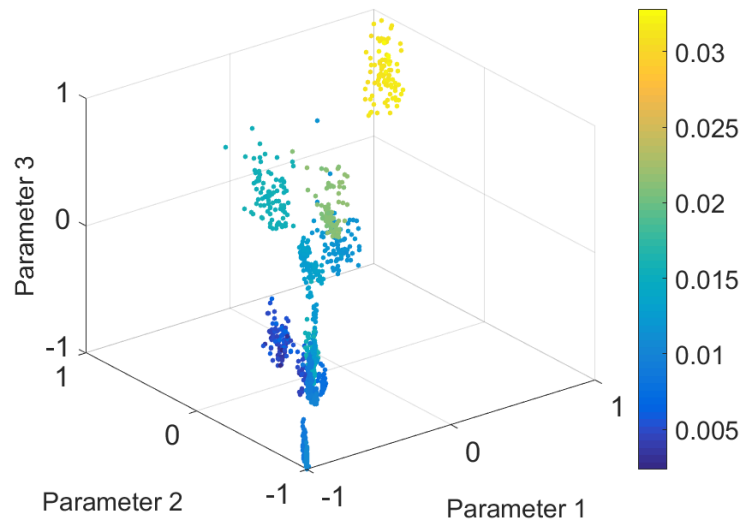

Figure 13. Surface clustering and multidimensional visualization in a 3D space.
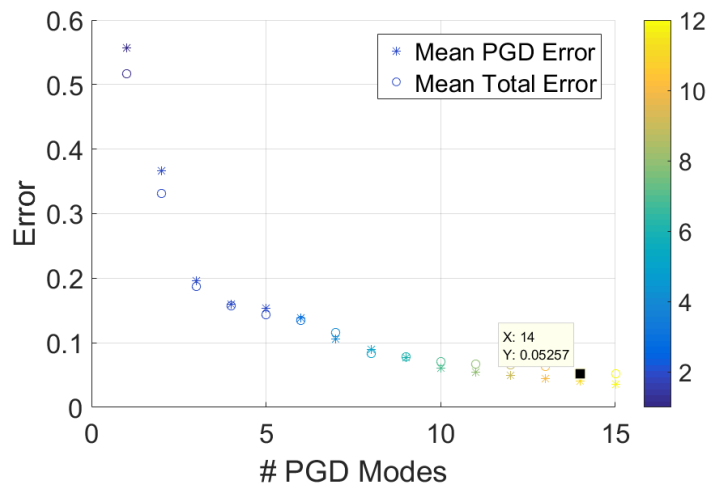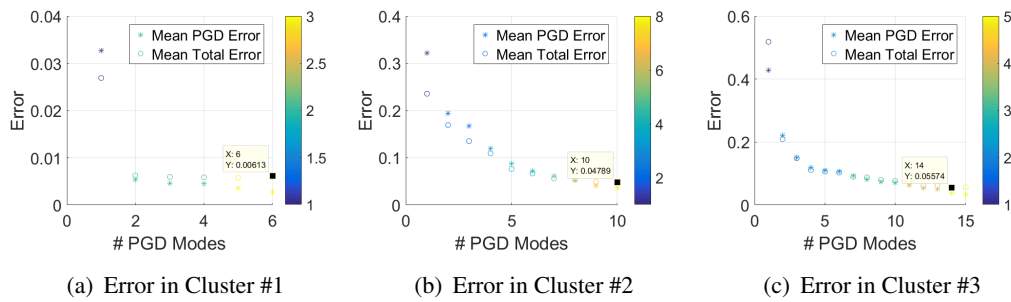

Figure 14. Error when using sPGD-based approximation with 50% of the surfaces for defining the regression model.

Now, taking into account that surfaces exhibit a noticeable clustering, as previously discussed and seen in Figure 13, we could define a sPGD operating at each cluster level. First using the k-means technique and the macro-curvature that is expected having the more important effect on the intimate contact evolution, surfaces were grouped in the three clusters depicted in Figure 15.

When applying local sPGD approximation at the level of each cluster the error reduces significantly as Figure 16 proves.

(a) Cluster 1: yellow points   (b) Cluster 2: yellow points   (c) Cluster 3: yellow points
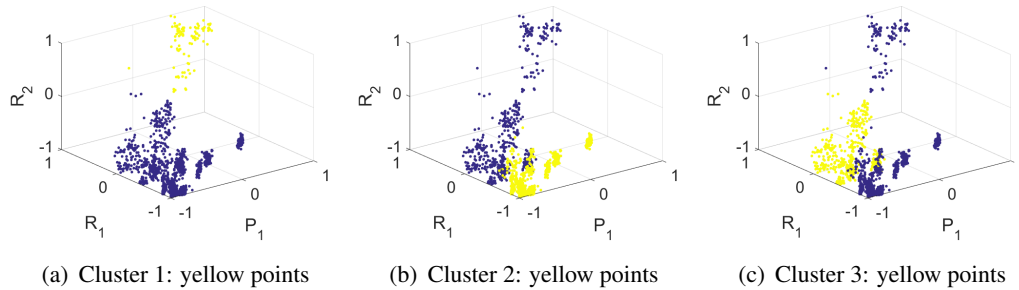
Figure 15. Surface clusters in which the local sPGD applies.

(a) Error in Cluster #1   (b) Error in Cluster #2   (c) Error in Cluster #3

Figure 16. Error evolution in each cluster for estimating the data that served to construct the model (Mean PGD Error) and the total set of data (Mean Total Error).

5. Conclusions

The main aim of the present work was to efficiently predict composite processability by evaluating the intimate contact from few geometrical parameters easily accessible. From a data-base consisting of thousands surface profiles, consolidation was simulated by solving numerically, by using the PGD, the heating and squeeze flow coupled problem. Curvature was expected to be of major relevance in the process. Data-mining techniques allowed to confirm this expectation and also to create a regression model relating the output of interest (the crushing time at which the contact becomes almost perfect) with a set of five geometrical parameters. Tree-based regression was considered for that purpose, and the evaluated error between the estimated crushing time and of the simulated one amounts to 5%, which proves the potential of the proposed approach.

Another route with greater physical significance was implemented, the one consisting of a nonlinear regression based on a multidimensional polynomial approximation. In order to address the two main issues encountered, first the sparse available data in the parametric space and second its multidimensional nature, we propose a sparse variant of the PGD-based approximation that when combined with an adaptive kriging approximation in the different parametric dimensions allowed accuracies of the same order of magnitude than the ones obtained by using tree-based regression.

Moreover, the accuracy was enhanced when considering local sPGD-based nonlinear regression at the level of surface clusters, the last constructed by making use of a classification strategy (e.g., k-means) with respect to the output of interest (here the crushing time).

Conflict of interest

No potential conflict of interest was reported by the authors.

References

1. Chinesta F, Leygue A, Bognet B, et al. (2014) First steps towards an advanced simulation of composites manufacturing by automated tape placement. *Int J Mater Form* 7: 81–92.

2. Chinesta F, Ammar A, Cueto E (2010) Recent advances and new challenges in the use of the Proper Generalized Decomposition for solving multidimensional models. *Arch Comput Method Eng* 17: 327–350.

3. Chinesta F, Ladeveze P, Cueto E (2011) A short review in model order reduction based on Proper Generalized Decomposition. *Arch Comput Method Eng* 18: 395–404.

4. Chinesta F, Keunings R, Leygue A (2014) *The Proper Generalized Decomposition for advanced numerical simulations. A primer*, Springer International Publishing.

5. Chinesta F, Ladeveze P (2014) *Separated representations and PGD based model reduction: Fundamentals and applications*, CISM-Springer.

6. Chinesta F, Huerta A, Rozza G, et al. (2016) Model Order Reduction, In: *Encyclopedia of Computational Mechanics*, 2Eds., Wiley.

7. Bognet B, Leygue A, Chinesta F, et al. (2012) Advanced simulation of models defined in plate geometries: 3D solutions with 2D computational complexity. *Comput Method Appl M* 201: 1–12.

8. Bognet B, Leygue A, Chinesta F (2014) Separated representations of 3D elastic solutions in shell geometries. *Adv Model Simul Eng Sci* 1: 4.

9. Bordeu F, Ghnatios Ch, Boulze D, et al. (2015) Parametric 3D elastic solutions of beams involved in frame structures. *Adv Aircr Spacecr Sci* 2: 233–248.

10. Ghnatios Ch, Chinesta F, Binetruy Ch (2015) The squeeze flow of composite laminates. *Int J Mater Form* 8: 73–83.

11. Chinesta F, Leygue A, Bordeu F, et al. (2013) Parametric PGD based computational vademecum for efficient design, optimization and control. *Arch Comput Method Eng* 20: 31–59.

12. Lee W, Springer G (1987) A model of the manufacturing process of thermoplastic matrix composites. *J Compos Mater* 21: 1057–1082.

13. Levy A, Heider D, Tierney J, et al. (2014) Inter-layer thermal contact resistance evolution with the degree of intimate contact in the processing of thermoplastic composite laminates. *J Compos Mater* 48: 491–503.

14. Coy J, Sidik S (1979) Two-dimensional random surface model for asperity contact in elastohydrodynamic lubrication. *Wear* 57: 293–311.

15. Longuet-Higgins M (1957) Statistical properties of an isotropic random surface. *Philos T R Soc A* 250: 157–174.

16. Longuet-Higgins M (1957) The Statistical Analysis of a Random, moving surface. *Philos T R Soc A* 249: 321–387.

17. Nayak P (1973) Some aspects of surface roughness measurement. *Wear* 26: 165–174.

18. Oden P, Majumdar A, Bhushan B, et al. (1992) AFM Imaging, roughness analysis and contact mechanics of magnetic tape and head surfaces. *J Tribol* 114: 666–674.

19. Sayles R, Thomas T (1976) Thermal conductance of a rough elastic contact. *Appl Energ* 2: 249–267.

20. Sayles R, Thomas T (1977) The spatial representation of surface roughness by means of the structure function: a practical alternative to correlation. *Wear* 42: 263–276.

21. Yaglom A (1987) *Correlation theory of stationary and related random function. Volume I: Basic Results*, New York: Springer-Verlag.

22. Borodich F, Mosolov A (1992) Fractal roughness in contact problems. *J Appl Math Mech* 56: 786–795.

23. Ganti S, Bhushan B (1995) Generalized fractal analysis and its applications to engineering surfaces. *Wear* 180: 17–34.

24. Mandelbrot B (1983) *The fractal geometry of Nature*, New York: W.H. Freeman and Company.

25. Mandelbrot B, Van Ness J (1968) Fractional Brownian motions, fractional noises and applications. *SIAM Rev* 10: 422–437.

26. Mandelbrot B, Passoja D, Paullay A (1984) Fractal character of fracture surfaces of metals. *Nature* 308: 721–722.

27. Mandelbrot B (2002) *Gaussian self-affinity and fractals*, New York: Springer-Verlag.

28. Majumdar A, Tien C (1990) Fractal Characterization and simulation of rough surfaces. *Wear* 136: 313–327.

29. Warren T, Majumdar A, Krajcinovic D (1996) A fractal model for the rigid-perfectly plastic contact of rough surfaces. *J Appl Mech* 63: 47–54.

30. Yang F, Pitchumani R (2001) A fractal cantor set based description of interlaminar contact evolution during thermoplastic composites processing. *J Mater Sci* 36: 4661–4671.

31. Leon A, Barasinski A, Nadal E, et al. (2015) High-resolution thermal analysis at thermoplastic pre-impregnated composite interfaces. *Compos Interface* 22: 767–777.

32. Leon A, Barasinski A, Chinesta F (2017) Microstructural analysis of pre-impregnated tapes consolidation. *Int J Mater Form* 10: 369–378.

33. Leon A, Argerich C, Barasinski A, et al. (2018) Effects of material and process parameters on in-situ consolidation. *Int J Mater Form* 1–13.

34. Saoudi A, Leon A, Gregoire G, et al. (2017) On the interfacial thermal properties of two rough surfaces in contact in preimpregnated composites consolidation. *Surf Topogr-Metrol* 5: 045010.

35. Helmus R, Kratz J, Potter K, et al. (2017) An experimental technique to characterize interply void formation in unidirectional prepregs. *J Compos Mater* 51: 579–591.

36. Leon A, Barasinski A, Abisset-Chavanne E, et al. (2018) Wavelet-based multiscale proper generalized decomposition. *CR Mecanique* 346: 485–500.

37. Dagnall H (2014) *Exploring Surface Texture*, Taylor Hobson Publishing Ltd.

38. Bhushan B (2001) *Modern Tribology Handbook*, CRC Press.

39. Torquato S (2002) Statistical Description of Microstructures. *Annu Rev Mater Res* 32: 77–111.